Journal of Thermal Analysis and Calorimetry (2023) 148:12467–12479
https://doi.org/10.1007/s10973-023-12552-z

MXene-wrapped zinc hydroxystannate nanocubes toward reducing the heat, smoke and toxicity hazards of ABS resin

Weihao Pan[1] · Qiankun Zhou[1] · Wenjie Yang[2] · Shibin Nie[3,4] · Liangji Xu[4] · Chunxiang Wei[1] · Hongdian Lu[1] · Wei Yang[1] · Anthony Chun Yin Yuen[5]

Received: 15 May 2023 / Accepted: 1 September 2023 / Published online: 28 September 2023

Abstract

Acrylonitrile–butadiene–styrene (ABS) composites with less smoke and toxicity hazards (e.g., HCN and NO_x) emission are highly demanded. As a common smoke suppressant, zinc hydroxystannate (ZHS) has been used in various polymers, while the high content, special cube shape and agglomeration restrict its development. To solve these problems, MXene ($Ti_3C_2T_x$) nanosheets were utilized to wrap ZHS nanoparticles ($Ti_3C_2T_x$-PDA-ZHS) to improve the dispersion and compatibility of ZHS nanoparticles in ABS, in which polydopamine (PDA) was used as a binder to combine ZHS and MXene nanosheets. Accordingly, the prepared ABS/$Ti_3C_2T_x$-PDA-ZHS nanocomposites showed the enhanced properties: (1) ABS/$Ti_3C_2T_x$-PDA-ZHS exhibited a 69.7% increase in elongation at break compared to ABS/ZHS at a 2 mass% loading. (2) Owing to the synergistic effect of MXene and ZHS, $Ti_3C_2T_x$-PDA-ZHS provided excellent inhibition on heat and toxic gas release during combustion (a reduction of approximately 17.5%, 34.5%, 19.1% and 20.0% of peak heat release rate, HCN, NO and NO_2, respectively). (3) The smoke density decreased from 525.6 for neat ABS to 423.2 for ABS/$Ti_3C_2T_x$-PDA-ZHS with a reduction of 19.5%, and the light transmittance of ABS/$Ti_3C_2T_x$-PDA-ZHS (37.7%) was much higher than that of pure ABS (21.2%) at 240 s. Therefore, $Ti_3C_2T_x$-PDA-ZHS showed a great enhancement in flammability, toxicity and smoke release reduction of ABS, potentially overcoming the weakness with improved diversity in future applications.

Weihao Pan and Qiankun Zhou contributed equally to this work (co-first author).

✉ Wei Yang
yangwei@hfuu.edu.cn

✉ Anthony Chun Yin Yuen
anthony-cy.yuen@polyu.edu.hk

[1] School of Energy, Materials and Chemical Engineering, Hefei University, 99 Jinxiu Avenue, Hefei 230601, Anhui, People's Republic of China

[2] Department of Architecture and Civil Engineering, City University of Hong Kong, Tat Chee Avenue, Kowloon, Hong Kong, People's Republic of China

[3] School of Safety Science and Engineering, Anhui University of Science and Technology, Huainan 232001, Anhui, People's Republic of China

[4] Institute of Energy, Hefei Comprehensive National Science Center (Anhui Energy Laboratory), Hefei 230041, Anhui, People's Republic of China

[5] Department of Building Environment and Energy Engineering, The Hong Kong Polytechnic University, Hung Hom, Kowloon, Hong Kong SAR, People's Republic of China

Graphical abstract

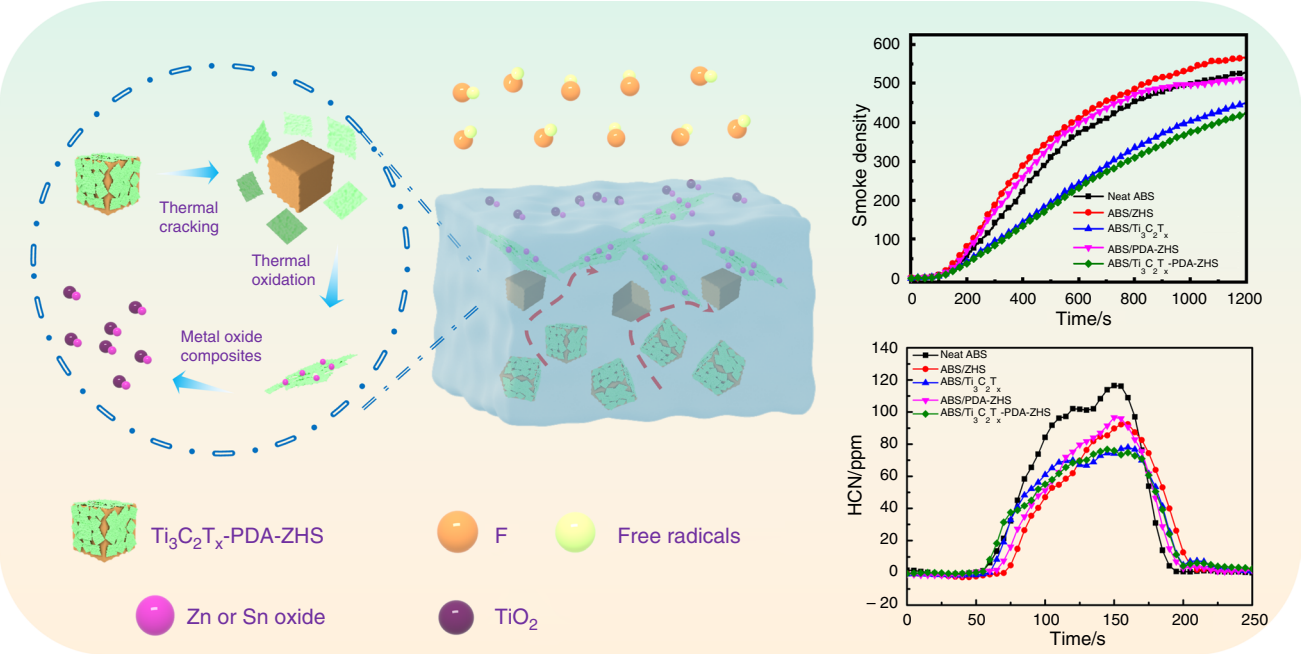

Keywords MXene · Zinc hydroxystannate · ABS resin · Smoke suppression · Toxicity hazards

Introduction

Acrylonitrile–butadiene–styrene (ABS) resin is one of the most widely used engineering thermoplastic polymers, which shows an uprising trend of applications in the automobile industry owing to its lightweight and rigid characteristics [1, 2]. As a terpolymer, ABS possesses excellent impact resistance, chemical resistance and electrical properties. Nonetheless, the major drawback of ABS is its highly flammable and toxic nature. It releases vast amounts of highly toxic compounds during combustion, including HCN and NO_x gases, producing lots of smoke, reducing visibility, making people unable to escape and causing environmental pollution [3]. Thus, it is necessary to improve the flame-retardant and smoke suppression properties of ABS to further expand its application fields.

Over the past decades, numerous efforts have been devoted to enhancing the fire, toxicity and smoke suppression of ABS through the incorporation of flame retardants, including halogen-based flame retardants [4], phosphorus-based flame retardants [5–10], polymer [11, 12], nanomaterials [13–18], etc. Among them, nanomaterials have attracted more attention due to their high efficiency and low loading. Besides, several unique structures such as carbon nanotubes and graphene nanosheets can endow polymers with improved flame retardancy and mechanical properties. For example, the addition of layered double hydroxide ZnMgAl-LDH to ABS significantly reduced the peak heat release rate (PHRR) from 489 to 214 kW m^{-2}, benefiting from the barrier effect of the exfoliated or intercalated LDH layer on the diffusion of oxygen into the heated polymer [15]. Du et al. [19] prepared ABS composites via octadecylamine-modified montmorillonite, resulting in a 42% reduction on PHRR for ABS composites compared to pure ABS. Nanotubes also play a significant role in the flame and smoke suppression of ABS. Ma et al. [14] grafted the intumescent flame-retardant polydiaminodiphenylmethane spirocyclopentetrol diphosphonate (PDSPB) onto the surface of carbon nanotubes (CNTs). The grafting of PDSPB improves the dispersion of CNTs in ABS. As the lattice structure of CNTs can reduce the flammable volatiles from polymer degradation during combustion, the nanocomposites obtained excellent flame retardancy (50% reduction in PHRR at 0.2 mass% loading). In addition, graphene has also been utilized to enhance the flame and smoke suppression properties of ABS. Traditionally, graphene has been modified with a range of phosphorus-, bromine- and metal-based compounds to enhance the dispersion of graphene in polymer matrix. Compared to unmodified graphene, the incorporation of modified graphene resulted in more significant reduction of heat release and toxic fumes of ABS owing to the synergistic catalytic effect between the modifiers and the graphene [20–25].

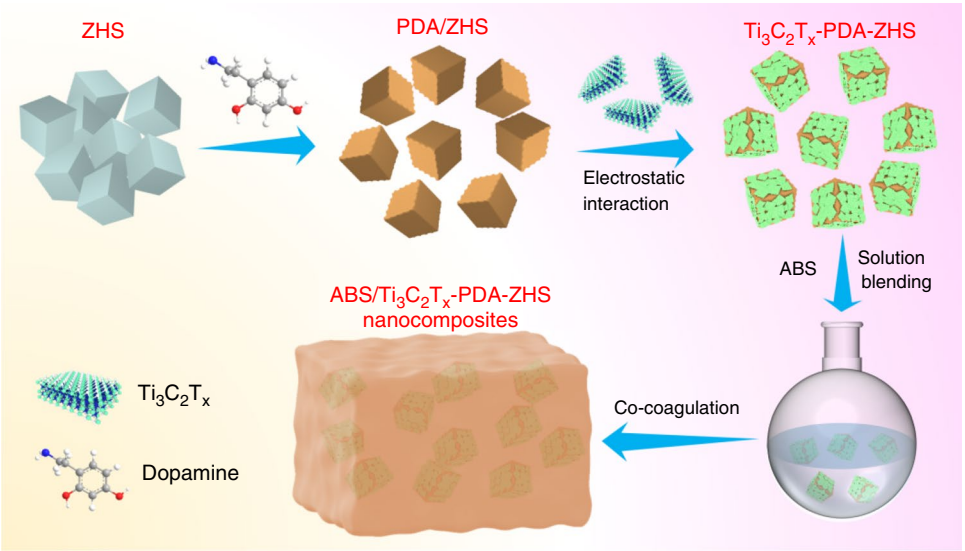

Scheme 1 Preparation process of ABS/$Ti_3C_2T_x$-PDA-ZHS nanocomposites

Zinc hydroxystannate (ZHS) is a traditional smoke suppressant used in polymers such as polyvinyl chloride and epoxy resins [26, 27], as Zn and Sn elements can form metal oxides which attach to the polymer surface during combustion, achieving a catalytic smoke suppression effect [28]. However, the sharp cubic morphology of ZHS always leads to negative compatibility when added into polymers. Besides, unmodified ZHS is prone to agglomeration, which further influences the dispersion of ZHS in polymers [29–32]. Therefore, pure ZHS may not endow polymers with good fire resistance, and it is often combined with other flame retardants to achieve a better fire and smoke suppression effect. In addition, the sharp cubic morphology of ZHS leads to the attenuation of mechanical properties of polymers.

$Ti_3C_2T_x$ (MXene), a recently discovered two-dimensional (2D) nanomaterial, is composed of transition metal carbides, nitrides or carbon nitrides of several atomic layers thicknesses (e.g., Ti_3C_2, Ti_2C, Nb_2C, V_2C, Ti_3CN and Mo_2C). The synthesis of $Ti_3C_2T_x$ is commonly conducted via etching the A-layer from the MAX phase (chemical general formula $M_{n+1}AX_n$). The relatively rich surface functional groups (–OH, –COOH) of $Ti_3C_2T_x$ provide the basis for surface engineering work [33, 34]. The use of $Ti_3C_2T_x$ as a nano-additive for preparing polymer nanocomposites with flame-retardant and smoke suppress properties has been extensively investigated. In our previous work, dipyridylmethylene boron (BODIPY)-modified $Ti_3C_2T_x$ nanosheets were prepared. Benefiting from the synergistic effect between BODIPY and $Ti_3C_2T_x$, the PHRR and peak smoke production rate (PSPR) of ABS presented an obvious reduction during combustion even at 0.5 mass% loading. The release of various toxic gases were significantly inhibited [35].

Therefore, utilizing MXene nanosheets to wrap ZHS is a potential method to enhance the compatibility between ZHS and polymers. To realize the encapsulation, poly(dopamine) (PDA) has been used as a binder to combine ZHS and $Ti_3C_2T_x$ via electrostatic adsorption between the protonated amino groups in dopamine and $Ti_3C_2T_x$ containing negative charge (Scheme 1) [35]. The prepared nanoparticles can minimize the negative effect of ZHS on the mechanical properties of ABS. In addition, the synergistic effect between $Ti_3C_2T_x$ and ZHS can effectively improve the flame-retardant efficiency and smoke emission of ABS, thus expanding its future development prospects.

Experimental

Materials

ABS resin (AG15A1) was supplied by Taiwan Petrochemical Industry. Zinc sulfate heptahydrate ($ZnSO_4{\cdot}7H_2O$) was obtained by Shanghai Zhanyun Chemical Co., Ltd. Sodium stannate trihydrate ($Na_2SnO_6{\cdot}3H_2O$) and dopamine hydrochloride (98%) were purchased from Shanghai Macklin Biochemical Co. Ltd. Titanium aluminum carbide (Ti_3AlC_2, 98%) was purchased from 11 Technology Co., Ltd. Changchun, China. Lithium fluoride (LiF, AR, 99%) and *N*, *N*-dimethylformamide (DMF, AR, 99.8%) were supplied by Aladdin Reagent Co. Ltd., China. Hydrochloric acid (HCl, 36.0–38.0 mass%) was purchased from Sinopharm Chemical Reagents Co. Ltd., Shanghai, China.

Preparation of PDA-ZHS

Firstly, 0.6 g of $ZnSO_4 \cdot 7H_2O$ and 0.6 g of $Na_2SnO_6 \cdot 3H_2O$ were dissolved in 300 mL of deionized water and stirred for 4 h. The precipitate was obtained via centrifugation and dried in an oven at 60 °C to obtain pure ZHS. 0.5 g of ZHS was uniformly dispersed by ultrasonication in 100 mL of Tris–HCl solution (10 mmol, pH 8.5). 0.2 g of dopamine hydrochloride was dissolved in a small amount of Tris–HCl solution and slowly added dropwise to the ZHS solution by using a dropper and stirred at room temperature for 24 h to obtain a dark brown solution. Finally, the resulting liquid was centrifuged to collect the precipitate, washed at least four times with water and dried at 60 °C to obtain a brown powder (PDA-ZHS).

Preparation of $Ti_3C_2T_x$-PDA-ZHS

The PDA-ZHS powder was dispersed in a small amount of deionized water, and the pH was adjusted to 1 by adding HCl solution. The acidified PDA-ZHS solution was dropped into the $Ti_3C_2T_x$ dispersion, and the precipitation in the solution indicated that PDA-ZHS was successfully attached to $Ti_3C_2T_x$ nanosheets (the mass ratio of PDA-ZHS to $Ti_3C_2T_x$ was 1:1). The precipitate was collected by centrifugation, washed neutrally and freeze-dried to obtain a black solid $Ti_3C_2T_x$ -PDA-ZHS [36–38].

Preparation of ABS/$Ti_3C_2T_x$-PDA-ZHS nanocomposites

The phase transformation method was used to prepare ABS/$Ti_3C_2T_x$-PDA-ZHS nanocomposites (Scheme 1). The dried $Ti_3C_2T_x$-PDA-ZHS powder was dispersed in DMF and sonicated for 1 h, and ABS particles were slowly added into the solution and stirred for 6 h after sonication for 1 h. The loading of $Ti_3C_2T_x$-PDA-ZHS was 2 mass% in the total mass of powder and ABS plastic. The obtained mixed solution was poured into deionized water in batches for phase conversion, and the resulting precipitate was dried in an oven at 60 ℃ to obtain ABS/$Ti_3C_2T_x$-PDA-ZHS composites. Meanwhile, ABS-ZHS, ABS/PDA-ZHS and ABS/$Ti_3C_2T_x$ composites were prepared by using the same method with the same additive loading (2 mass%).

Characterizations

X-ray diffraction (XRD) was used to investigate the structure of nanomaterials and char residues based on an X-ray diffractometer (Rigaku Co., Japan) with Cu Kα radiation ($\lambda = 0.1542$ nm). Thermogravimetric analysis (TGA) was carried out via a TGA Q5000IR thermo-analyzer (TA Instruments Inc., USA) with a heating rate of 20 °C min^{-1} under N_2/air condition. The mass of each specimen was 5–10 mg. A transmission electron microscope (TEM) was used to observe the morphology of nanomaterials based on JEM-2100F. The morphology and mapping images of nanomaterial were recorded via Hitachi Regulus 8100.

The tensile properties of neat ABS and its nanocomposites were tested by a Universal Mechanical Testing Machine (YF-900, Yuanfeng Testing Equipment Co., Ltd., Yangzhou, China) with a 50 mm min^{-1} cross-speed. An average of five individual determinations was gained.

Limiting oxygen index (LOI) was determined by an HC-2 Oxygen Index instrument (Jiangning Analytical Instrument Co. Ltd., China) according to ASTM D2863-2008. A cone calorimeter coupled with FTIR (iCone Classic, Fire Testing Technology, UK) was employed to evaluate the burning behavior and toxicity hazards of neat ABS and ABS composites at an incident flux of 35 kW m^{-2}. Prior to testing, all the samples with dimensions of $100 \times 100 \times 3$ mm^3 were wrapped with aluminum foil. Smoke density tests were performed in an NBS chamber (VOUCH 5920, Suzhou Vouch Testing Technology Co. Ltd., China) according to ISO 5659. The sample with dimension of $75 \times 75 \times 3$ mm^3 was tested in the chamber with a heat flux of 25 kW m^{-2}. The residues of ABS nanocomposites after calcination under air were analyzed by using a SU8010 field emission SEM (FESEM, Japan) at an acceleration voltage of 10 kV, XRD (Rigaku Co., Japan) and Raman spectra (Laser confocal micro Raman spectrometer of Thermo Fisher, DXR, USA).

Results and discussion

Morphology and structure

XRD was used to characterize the structure of ZHS, $Ti_3C_2T_x$ and $Ti_3C_2T_x$-PDA-ZHS. As shown in Fig. 1a, all the main characteristic diffraction peaks are in good agreement with the ZHS in the cubic phase of the standard chalcogenide structure with the perovskite structure (JCPDS: NO. 74-1825), indicating the successful synthesis of ZHS. The characteristic diffraction peaks of the PDA-coated ZHS exhibit no obvious difference from those of pure ZHS because PDA shows an amorphous state. In addition, the XRD pattern of $Ti_3C_2T_x$-PDA-ZHS demonstrates a similar characteristic diffraction peak to that of pure ZHS and $Ti_3C_2T_x$, indicating the successful formation of $Ti_3C_2T_x$-PDA-ZHS [39].

Figure 1b shows the thermal stability of ZHS, PDA, PDA-ZHS, $Ti_3C_2T_x$ and $Ti_3C_2T_x$-PDA-ZHS under nitrogen atmosphere. It can be seen that ZHS presents one-step decomposition with a higher char yield compared with PDA-ZHS. PDA exhibits a high decomposition temperature with the lowest char residue, which means that most of PDA decomposes

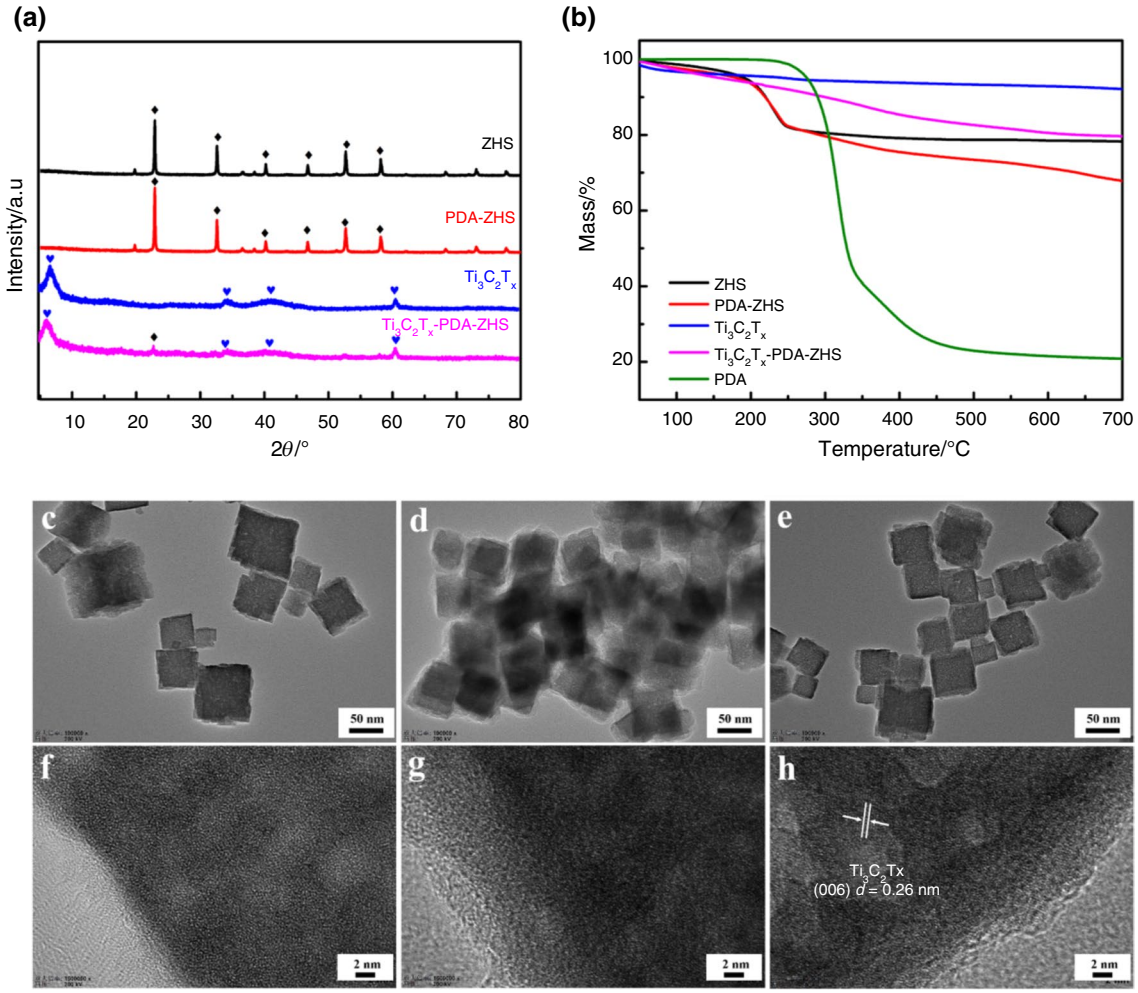

Fig. 1 XRD patterns (**a**); TGA curves (**b**); TEM images (**c**–**h**) of different nanoparticles: ZHS (**c**, **f**), PDA-ZHS (**d**, **g**), $Ti_3C_2T_x$-PDA-ZHS (**e**, **h**)

during the heating process. However, PDA-ZHS exhibits similar decomposition curves with ZHS during the first decomposition process, indicating that PDA has no fundamental influence on the thermal stability of ZHS. Besides, the continued mass loss is due to the decomposition of PDA. In addition, the thermal stability of the pure $Ti_3C_2T_x$ sheet is the best in all samples, and no significant mass loss can be seen during the heating process. When PDA-ZHS is wrapped by $Ti_3C_2T_x$, $Ti_3C_2T_x$-PDA-ZHS results in continued mass loss throughout the heating process. As the PDA decomposes, $Ti_3C_2T_x$ nanosheets may fall off from the ZHS surface.

The surface morphology of the nanoparticles was characterized by TEM (Fig. 1c–h). Pure ZHS presents a cubic morphology with sharp edges. Its diameter ranges from 20 to 100 nm. After coating with PDA, the ZHS starts becoming mellow and smooth, which may be helpful to improve the dispersion of ZHS in ABS. Subsequently, after being coated with $Ti_3C_2T_x$, the lattice striations (006) of $Ti_3C_2T_x$ are observed in Fig. 1h [40]. The result can be confirmed by element mapping images (Fig. S1), in which the specific elements such as Ti, N, Sn and Zn are observed. Combined with the results of XRD and TGA, it can be proven that the surface of PDA-ZHS is sufficiently wrapped by $Ti_3C_2T_x$ to form $Ti_3C_2T_x$-PDA-ZHS nanohybrids.

Thermal decomposition behaviors

The thermal stability of ABS and its nanocomposites under N_2 and air conditions is shown in Fig. 2 and Table S1, including the initial decomposition temperature ($T_{-5\%}$), maximum decomposition temperature (T_{max}) and char yield at 700 °C (CY_{700}). Figure 2a shows that under nitrogen conditions, pure ABS decomposes at 384 °C with a 1.1% char yield. It indicates that ABS has poor carbon formation property, resulting in the release of large amounts of heat and toxic gases during thermal decomposition and combustion. With the addition of

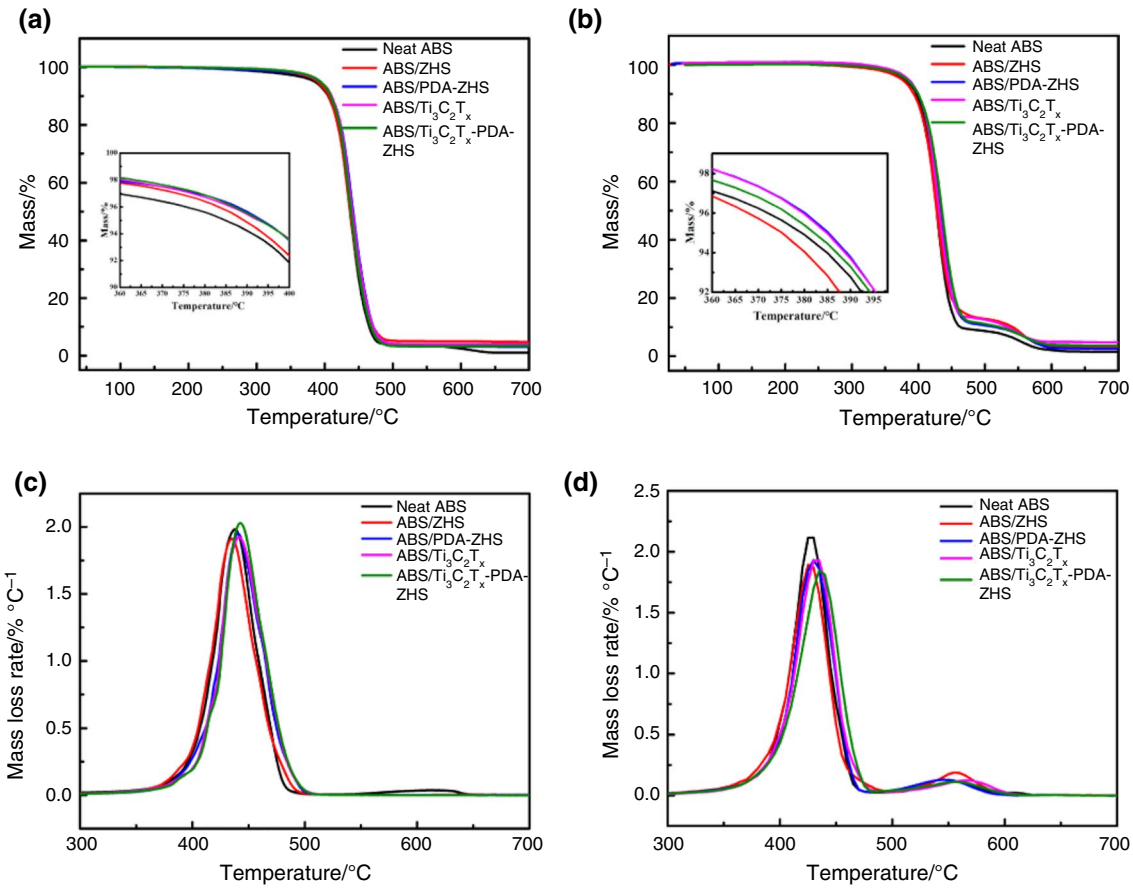

Fig. 2 TGA and DTG curves of neat ABS and ABS composites under N_2 (**a**, **c**) and air (**b**, **d**) condition

nanomaterials, the initial thermal decomposition temperature of several composites increases from 389 to 393 °C, which is higher than that of pure ABS. The reason can be attributed to the high thermal stability of ZHS and $Ti_3C_2T_x$. In addition, ZHS and $Ti_3C_2T_x$ show a better catalytic carbon formation property for ABS, as CY_{700} increases from 1.1% for ABS to 3.3% for ABS/$Ti_3C_2T_x$-PDA-ZHS. It further confirms that ZHS and $Ti_3C_2T_x$ can increase the thermal protection of the underlying matrix against fire. Under air condition (Fig. 2c, d), the $T_{-5\%}$ for ABS, ABS/ZHS, ABS/$Ti_3C_2T_x$, ABS/PDA-ZHS and ABS/$Ti_3C_2T_x$-PDA-ZHS is 379 °C, 375 °C, 385 °C, 384 °C and 382 °C, respectively. It further verifies that the introduction of $Ti_3C_2T_x$-PDA-ZHS can enhance the thermal stability of ABS. As shown in Fig. 2d, ABS/$Ti_3C_2T_x$-PDA-ZHS presents the lowest decomposition rate compared with pure ABS and the other ABS nanocomposites due to the catalytic charring effect of $Ti_3C_2T_x$-PDA-ZHS. A stable carbon layer formed during thermal oxidation can prevent further decomposition of the ABS internal matrix.

Tensile properties

The previous studies revealed that the addition of pure ZHS into polymers showed a negative effect on the mechanical properties of the polymer due to the sharp shape of ZHS and the agglomeration of small particles in polymer matrix [30, 31, 41–46]. Therefore, ZHS wrapped by $Ti_3C_2T_x$ nanosheets may potentially resolve the agglomeration problem of ZHS and enhance the dispersion of ZHS in ABS. The stress–strain curves (Fig. 3) show that the tensile strength increases from 37.4 MPa for pure ABS to 40.7 MPa for ABS/ZHS. However, the strain decreases from 22.8 to 15.5% (Table S2). It can be ascribed to the sharp edges of ZHS, which leads to the formation of nano-gaps between ABS and ZHS, resulting in an increase in the brittleness of ABS. On the other hand, the dispersion of unmodified ZHS particles is probably influenced by the agglomeration of the nanoparticles, leading to a reduction of material properties (see Fig. S2). The elongation at break of ABS improves after the incorporation of PDA-ZHS, because the modification of PDA can reduce

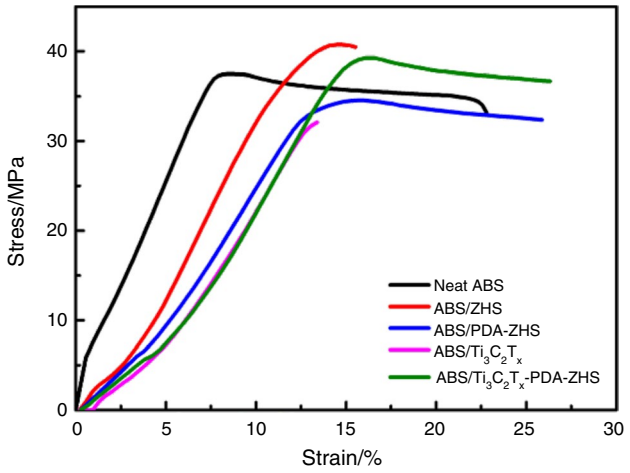

Fig. 3 Stress–strain curves of neat ABS and ABS nanocomposites

the negative effect of the sharp edges of ZHS and eliminate the nano-gaps. It indicates that using PDA to wrap ZHS can improve the compatibility between ABS and ZHS.

The stress and strain of ABS decrease significantly with the addition of $Ti_3C_2T_x$ due to the agglomeration of $Ti_3C_2T_x$ nanosheets within the ABS matrix, which results in a decrease in the mechanical properties of ABS. After the addition of $Ti_3C_2T_x$-PDA-ZHS, the tensile properties are largely improved with 69.7% enhancement of the elongation at break, while there is no obvious strength sacrifice, compared to ABS/ZHS. The improvement in mechanical properties can be attributed to the better dispersion of $Ti_3C_2T_x$-PDA-ZHS (Fig. S2). There is no obvious agglomeration of $Ti_3C_2T_x$-PDA-ZHS in ABS compared to pure ZHS, which further proves the viability of the modification of ZHS. Besides, when $Ti_3C_2T_x$ nanosheets are adhered to the surface of PDA-ZHS, the numerous functional groups on $Ti_3C_2T_x$, such as hydroxyl and carboxyl groups, can form strong intermolecular forces (i.e., hydrogen bonds) with the ABS molecular chains, thus improving the mechanical properties of ABS.

As shown in Table S3, the previously reported ZHS in polymers tends to show a negative impact on the mechanical properties of the materials, especially on the elongation at break, while $Ti_3C_2T_x$-PDA-ZHS effectively enhanced the mechanical properties of ABS, far exceeding the previously reported works. This work demonstrates that the negative effect of the special shape of ZHS on the mechanical properties of polymeric materials can be effectively addressed.

Flame retardancy and smoke density

The limiting oxygen index (LOI) testing results are shown in Table 1. It can be seen that the incorporation of $Ti_3C_2T_x$-PDA-ZHS into ABS leads to the slight improvement of LOI. The other additives have no fundamental influence on LOI. The cone calorimetry test (CCT) simulates real fire conditions and is widely used to assess the flammability and potential fire safety of polymeric materials with respect to parameters such as time to ignition (TTI), heat release rate (HRR), peak CO_2 production (PCO_2P), peak CO production (PCOP), total heat release (THR) and char residues [47–49]. In a fire, a lower peak heat release rate (PHRR) means higher fire safety. The HRR and THR curves for ABS and its composites are shown in Fig. 4a, b. The HRR curves show that the addition of $Ti_3C_2T_x$-PDA-ZHS to ABS results in a 17.5% reduction with a lowest PHRR value of 877.1 kW m^{-2} compared to 1062.9 kW m^{-2} for pure ABS. Besides, the PHRR of ABS/$Ti_3C_2T_x$-PDA-ZHS is also lower than that of ABS/ZHS (1103.7 kW m^{-2}), ABS/PDA-ZHS (1085.4 kW m^{-2}) and ABS/$Ti_3C_2T_x$ (904.1 kW m^{-2}), which may be the result of the synergistic effect between ZHS and $Ti_3C_2T_x$. For THR, there is no fundamental difference between the composites, which is due to the low loading of the additives that cannot efficiently improve the char yields.

In the past decades, researchers have found that the release of toxic gases and smoke is one of the most important causes of death and injury in fire accidents. In consequence, suppressing the release of toxic gases during combustion is vital. Figure 4 and Table 1 show a high PCOP of 0.028 g/s for pure ABS and 0.022 g/s for ABS/$Ti_3C_2T_x$-PDA-ZHS with a reduction of about 21.4%. The PCO_2P decreases from 0.77 g/s for pure ABS to 0.65 g/s for ABS/$Ti_3C_2T_x$-PDA-ZHS with a reduction of about 15.6%. This is mainly due to the synergistic effect of ZHS and $Ti_3C_2T_x$. The oxidation of ZHS can produce metal oxides which act as a barrier to the release of smoke, while $Ti_3C_2T_x$ plays a catalytic role internally to produce TiO_2 to achieve the effects of smoke reduction and suppression. To further evaluate the suppression of toxic gas volatile releases, FTIR real-time monitoring in the combustion was utilized to characterize the release of various toxicity volatiles. The detailed data are shown in Fig. 5 and Tables S4 and S5. For HCN, NO, NO_2, CO and CO_2, the curves present similar trends with the HRR curve of ABS and its nanocomposites. The control ABS shows the highest peak concentration and total release amount of toxic and asphyxiant gases compared to other nanocomposites. With the addition of ZHS, PDA-ZHS and $Ti_3C_2T_x$, there are reductions in peak values. The addition of PDA-ZHS and ZHS results in almost identical improvements in ABS smoke suppression performance, indicating that there is no significant synergistic effect between PDA and ZHS. ABS/$Ti_3C_2T_x$-PDA-ZHS exhibits the lowest values of HCN, NO and NO_2 compared to pure ABS (approximately 34.5%, 19.1% and 20.0% reduction, respectively), indicating that the addition of $Ti_3C_2T_x$ and ZHS has a better flame and smoke suppression effect. In addition, the wrapping of $Ti_3C_2T_x$ further enhances the dispersion of ZHS in

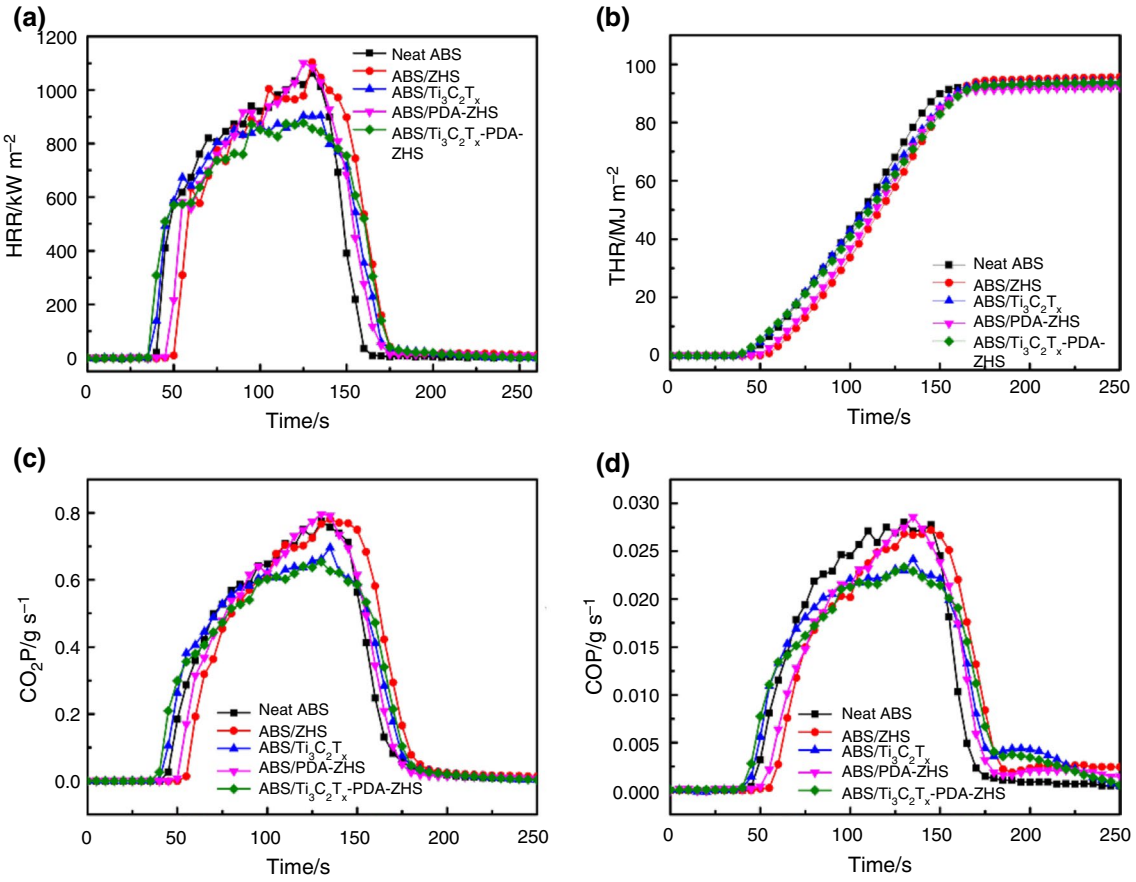

Fig. 4 HRR (**a**), THR (**b**), CO_2 (**c**), CO (**d**) as a function of the burning time for ABS and its nanocomposites

Table 1 The CCT and LOI results of ABS and its nanocomposites

Sample	TTI/s	PHRR/kW m^{-2}	THR/MJ m^{-2}	PCO$_2$P/g s^{-1}	PCOP/g s^{-1}	LOI/%
Error	±2	±30	±0.5	±0.02	±0.005	±0.5
ABS	42	1062.9	92.5	0.77	0.028	20
ABS/ZHS	50	1103.7	95.9	0.78	0.027	21
ABS/Ti$_3$C$_2$T$_x$	38	904.1	94.1	0.69	0.024	21
ABS/PDA-ZHS	48	1085.4	92.3	0.79	0.028	21
ABS/Ti$_3$C$_2$T$_x$-PDA-ZHS	39	877.1	93.6	0.65	0.022	21.5

LOI, limiting oxygen index; TTI, time to ignition; PHRR, peak heat release rate; THR, total heat release; PCO2P, peak CO2 production; PCOP, peak CO production

ABS and improves its compatibility with ABS to achieve the best flame-retardant and smoke suppressing effect.

Smoke density can identify the amount of smoke emitted by a material, which is described by the amount of light intensity attenuation through the smoke. The larger smoke density means that more smoke is released during combustion, which is detrimental to evacuating people and extinguishing fires, affecting the safety of people's lives and property [50–52]. Flammable materials produce large amounts of toxic smoke and soot during combustion. The suppression of the smoke production behavior of ABS by $Ti_3C_2T_x$-PDA-ZHS was assessed by smoke density testing. Figure 6 shows the variation in transmittance and smoke density over time. In general, the best escape time in a fire is 2–3 min [52, 53]. It means that 240 s may be an ultimate escape time. As shown in Fig. 6a, the light transmittance of ABS is 21.2% at 240 s, while the light transmittance of ABS is reduced after the incorporation of ZHS and PDA-ZHS. It means that the presence of ZHS in ABS improves the smoke emissions. Surprisingly, the light transmittance of ABS/$Ti_3C_2T_x$-PDA-ZHS increases to 37.7% after the introduction of $Ti_3C_2T_x$ to ZHS (higher than the 34.0%

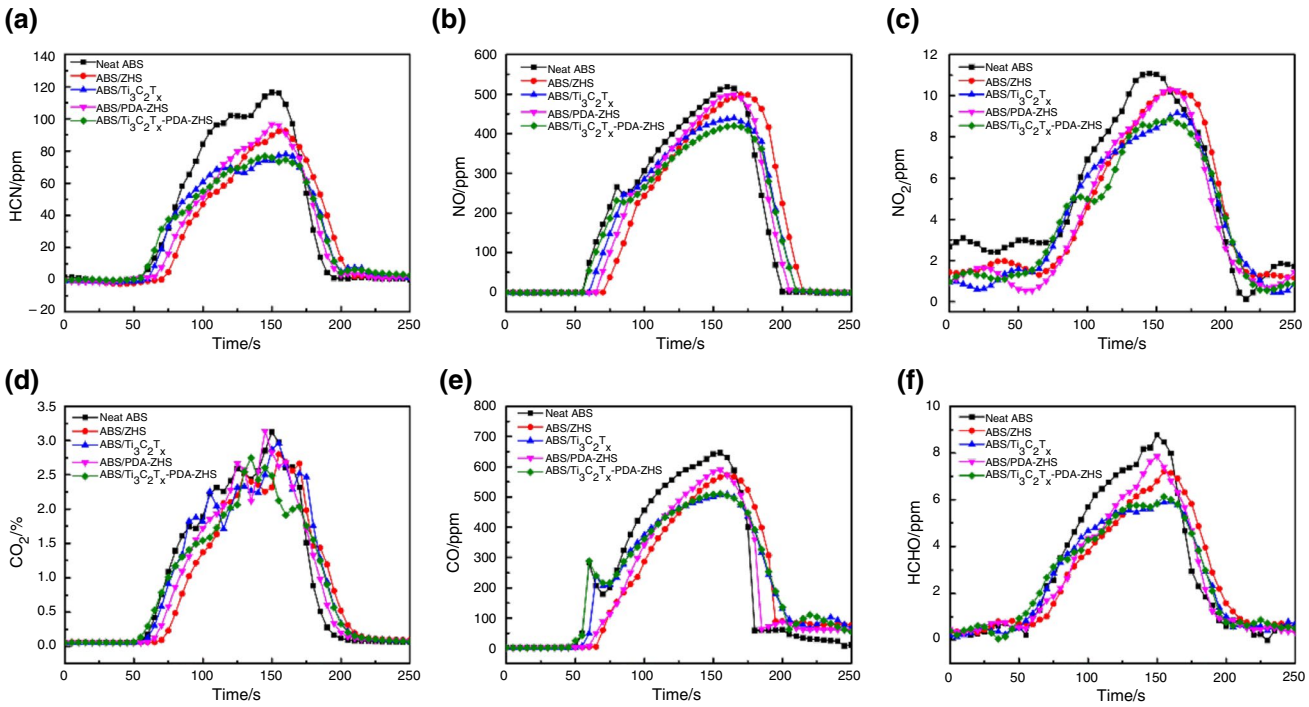

Fig. 5 FTIR gas analysis of ABS and its nanocomposites

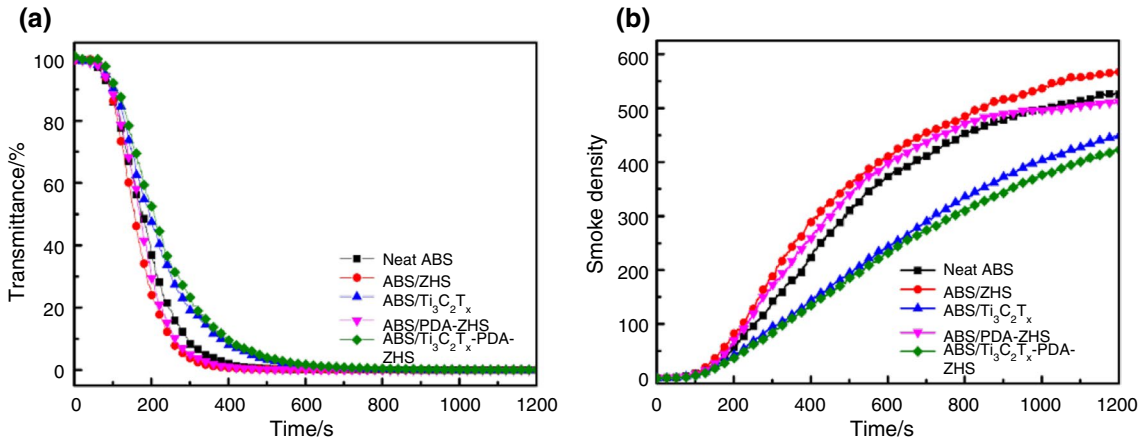

Fig. 6 Transmittance (**a**) and smoke density (**b**) as a function of the burning time for ABS and nanocomposites

of ABS/$Ti_3C_2T_x$). It indicates that there is a good synergy between ZHS and $Ti_3C_2T_x$ for the smoke suppression performance of ABS [54]. In Fig. 6b, the smoke density of ABS reaches to 525.6 at 1200 s. The smoke density of ABS/$Ti_3C_2T_x$-PDA-ZHS is 423.2 at 1200 s, which is lower than that of ABS/$Ti_3C_2T_x$, ABS/PDA-ZHS and ABS/ZHS. Compared to the ABS, the 19.5% reduction in smoke density indicates that the smoke production of ABS/$Ti_3C_2T_x$-PDA-ZHS is significantly reduced during combustion. Therefore, based on the above results, $Ti_3C_2T_x$-PDA-ZHS is an excellent nano-flame-retardant and smoke suppressant material, which also helps to inhibit the release of toxic gases to better protect people's lives and property in case of fire.

Flame-retardant mechanism

The flame-retardant mechanism of ABS composites can be clarified on the basis of gas- and condensed-phase analysis. In the gas phase, the release of gas volatiles is indicative of combustion. As illustrated in Fig. 5, $Ti_3C_2T_x$-PDA-ZHS inhibits CO and CO_2 more significantly than $Ti_3C_2T_x$ or ZHS. The peak concentration of toxic volatiles decreases

during combustion in ABS/$Ti_3C_2T_x$-PDA-ZHS and ABS/$Ti_3C_2T_x$ nanocomposites, which means that the volatiles are decreased, resulting in the reduction of PHRR. The reason can be explained as follows: (1) During the heating process, MXene nanosheets are exfoliated from $Ti_3C_2T_x$-PDA-ZHS. The barrier of MXene acts as a vital role on suppressing the migration of combustion volatiles, which results in the reduction of flammable gases [55]. (2) The radical trapping effect contributes to the improved flame retardancy, which is caused by the release of a large amount of fluorine-based volatiles into the gas phase during the decomposition of $Ti_3C_2T_x$-PDA-ZHS. As the halogen elements, fluorine-based volatiles may be involved in the free radical reactions and the barrier and catalytic effect of the $Ti_3C_2T_x$ nanosheets prolong the residence time of the fluorine atoms in the flame region. As a result, more "hot" radicals are removed from ABS.

The char residues were characterized by SEM, Raman spectra and XRD (Fig. 7). The SEM images show that the surface of ABS/ZHS is irregular, and there are many cracks with different sizes, which facilitate the emission of heat and smoke during combustion. The SEM images of the char residues of ABS/$Ti_3C_2T_x$ and ABS/$Ti_3C_2T_x$-PDA-ZHS show a flat surface, which is helpful for blocking the emission of toxic smoke. Figure 7d–f presents the Raman spectra of ABS/ZHS, ABS/$Ti_3C_2T_x$ and ABS/$Ti_3C_2T_x$-PDA-ZHS. All samples show two major peaks at approximately 1365 cm^{-1} (D band) and 1590 cm^{-1} (G band). The degree

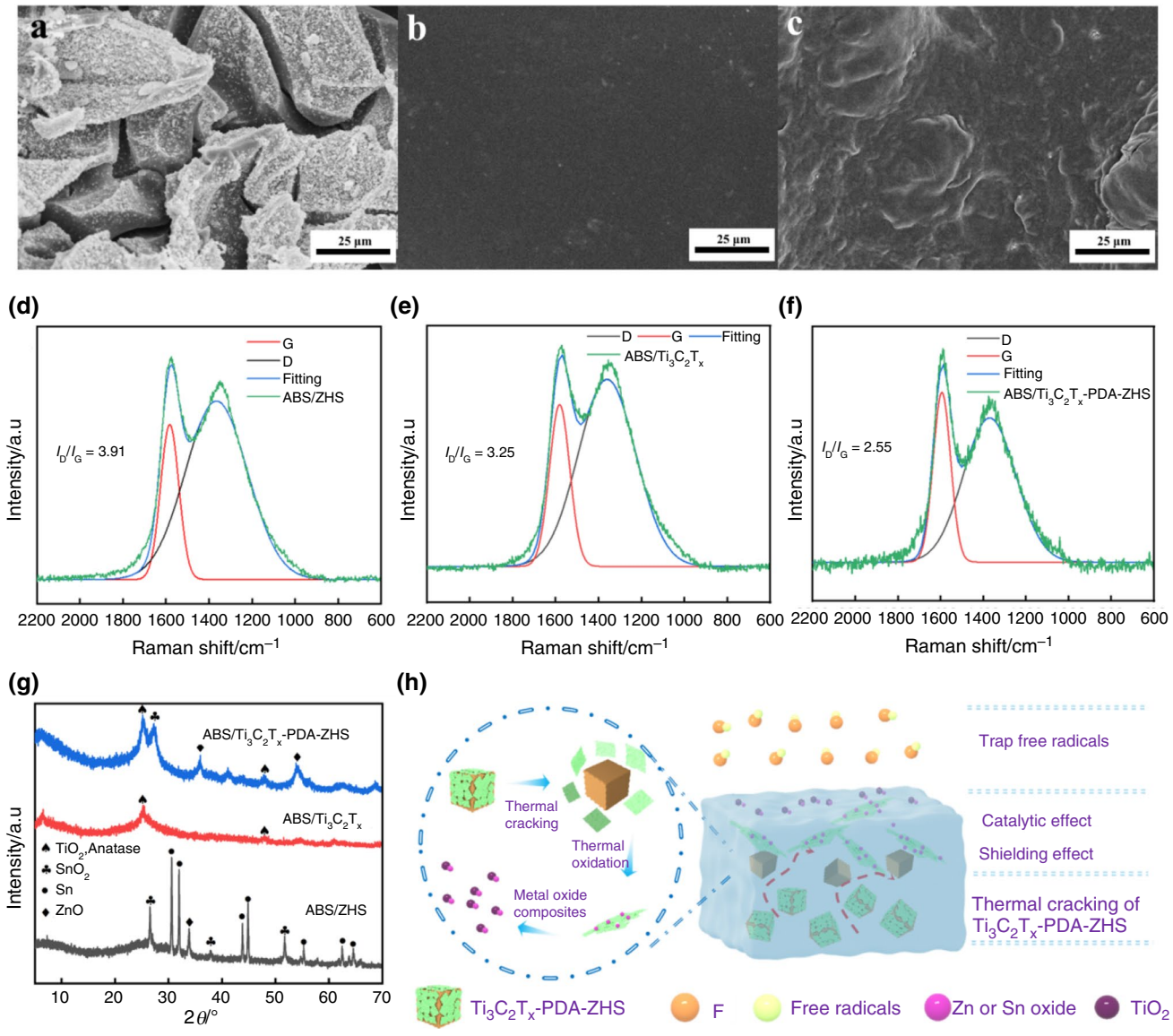

Fig. 7 SEM images (**a**–**c**) and Raman (**d**–**f**) spectra of the corresponding residues for ABS/ZHS (**a**, **d**), ABS/$Ti_3C_2T_x$ (**b**, **e**), ABS/$Ti_3C_2T_x$-PDA-ZHS (**c**, **f**); schematic flame-retardant mechanism (**h**)

of graphitization of the residues was calculated based on the ratio of the integrated intensity of the D/G band (I_D/I_G), which determines the stability of the chars. The lower I_D/I_G value indicates a higher degree of graphitization [48, 56, 57]. The I_D/I_G of ABS/ZHS and ABS/$Ti_3C_2T_x$ is 3.91 and 3.25, while ABS/$Ti_3C_2T_x$-PDA-ZHS shows the lowest I_D/I_G value (2.55). It demonstrates that the char residues with higher graphitization are formed due to the excellent synergistic catalytic effect between ZHS and $Ti_3C_2T_x$. The char residues are more mechanically and thermally stable, which is more effective in suppressing flame spread, melting and dripping of ABS. Moreover, the char residues were ground into a powder for XRD characterization. From Fig. 7g, it is found that the chars from ABS/$Ti_3C_2T_x$-PDA-ZHS clearly show lattice peaks of TiO_2, ZnO and SnO_2. It has been proven that MXene is oxidized into TiO_2-based nanosheets [58], which can present the positive effect on the char formation process. The compounds composed of ZnO and SnO_2 are generated from the degradation of ZHS. Thus, the ternary metal catalytic effect on the combustion and smoke emission of the composites leads to the formation of more stable char layers [58, 59] (Fig. 7g).

The flame-retardant mechanism of $Ti_3C_2T_x$-PDA-ZHS in ABS can therefore be summarized as follows (Fig. 7h): In the condensed phase, the PDA gradually decomposes at the beginning of combustion, causing the $Ti_3C_2T_x$ flakes to gradually fall off from the top of the ZHS, and the "tortuous path" effect can suppress the smoke release [55]. Besides, the ternary metal catalytic effect might contribute to the formation of more mechanically and thermally stable char residues, which inhibit the emission of toxic smoke and flammable volatiles. In the gas phase, $Ti_3C_2T_x$ emits F atoms to trap the free radicals released by ABS combustion, blocking the chain reaction of ABS and reducing the concentration of flammable volatiles. Thus, it can accelerate the self-extinguishing process and reduce the heat release of ABS during combustion.

Conclusions

In this work, a series of ABS nanocomposites with high efficiency in smoke and toxicity inhibition were prepared by facile attachment modification of ZHS. The results showed that the elongation at break of ABS/$Ti_3C_2T_x$-PDA-ZHS was 15.4% higher without any sacrifice of the tensile strength compared to pure ABS. The results demonstrated that the modification resulted in an ABS composite with an overall improvement in mechanical properties. In addition, ternary metal catalysis was effective in suppressing the release of toxic gas volatiles and smoke particulates during combustion. ABS/$Ti_3C_2T_x$-PDA-ZHS demonstrated peak value reductions of approximately 17.5%, 34.5%, 19.1% and 20.0% for PHRR, HCN, NO and NO_2, respectively. The smoke density decreased from 525.6 for neat ABS to 423.2 for ABS/$Ti_3C_2T_x$-PDA-ZHS, with a reduction of 19.5%, and the light transmittance of ABS/$Ti_3C_2T_x$-PDA-ZHS (37.7%) was much higher than that of pure ABS (21.2%) at 240 s. Hence, the potential overcoming of the major drawbacks of ABS in its high flammability and toxicity by incorporating modified ZHS will diversify the industry applications of ABS, potentially in the building and automobile sectors.

Appendix A. Supplementary data

Supplementary data associated with this article can be found in the online version.

Supplementary Information The online version contains supplementary material available at https://doi.org/10.1007/s10973-023-12552-z.

Acknowledgements This work was co-financed by the Anhui Provincial Natural Science Foundation for Distinguished Young Scholar (2008085J26), Natural Science Foundation in University of Anhui Province (KJ2021ZD0119 and 2022AH040251), University Synergy Innovation Program of Anhui Province (GXXT-2022-018), Excellent Scientific Research and Innovation Team in University of Anhui Province (2022AH010096 and 2023AH010050), Startup Fund for Distinguished Scholars in Hefei University (20RC37) and Anhui Provincial Natural Science Foundation (2108085QB47).

Author contributions All authors contributed to the study conception and design. Material preparation, data collection and analysis were performed by WP, QZ, WY, SN and LX. The first draft of the manuscript was written by WP and QZ. The manuscript was further revised and polished by CW, HL, WY and ACYY. All authors read and approved the final manuscript.

Declarations

Competing interest The authors have no relevant financial or nonfinancial interests to disclose.

References

1. Levchik SV, Weil ED. New developments in flame retardancy of styrene thermoplastics and foams. Polym Int. 2008;57:431–48.
2. Olivera SM, Venkatesh HB, Gopalakrishna K, Vivek K, Suryaprakash C. Plating on acrylonitrile–butadiene–styrene (ABS) plastic: a review. J Mater Sci. 2016;51:3657–74.
3. Prieur B, Meub M, Wittemann M, Klein R, Bellayer S, Fontaine G, Bourbigot S. Phosphorylation of lignin to flame retard acrylonitrile butadiene styrene (ABS). Polym Degrad Stabil. 2016;127:32–43.
4. Chen L, Wang Y-Z. A review on flame retardant technology in China. Part I: development of flame retardants. Polym Adv Technol. 2010;21:1–26.
5. Li J, Ke C, Xu L, Wang Y. Synergistic effect between a hyperbranched charring agent and ammonium polyphosphate on the

intumescent flame retardance of acrylonitrile-butadiene-styrene polymer. Polym Degrad Stab. 2012;97:1107–13.
6. Zhang Y, Chen X, Fang Z. Synergistic effects of expandable graphite and ammonium polyphosphate with a new carbon source derived from biomass in flame retardant ABS. J Appl Polym Sci. 2013;128:2424–32.
7. Ge L-L, Duan H-J, Zhang X-G, Chen C, Tang J-H, Li Z-M. Synergistic effect of ammonium polyphosphate and expandable graphite on flame-retardant properties of acrylonitrile-butadiene-styrene. J Appl Polym Sci. 2012;126:1337–43.
8. Realinho V, Haurie L, Formosa J, Velasco JI. Flame retardancy effect of combined ammonium polyphosphate and aluminium diethyl phosphinate in acrylonitrile-butadiene-styrene. Polym Degrad Stab. 2018;155:208–19.
9. Wu N, Li X. Flame retardancy and synergistic flame retardant mechanisms of acrylonitrile-butadiene-styrene composites based on aluminum hypophosphite. Polym Degrad Stab. 2014;105:265–76.
10. Hoang D, Kim W, An H, Kim J. Flame retardancies of novel organo-phosphorus flame retardants based on DOPO derivatives when applied to ABS. Macromol Res. 2015;23:442–8.
11. Attia NF. Green synthesis of polymer nanofibers and their composites as flame-retardant materials for polymer nanocomposites. Polym Adv Technol. 2016;27:1091–7.
12. Attia NF. Organic nanoparticles as promising flame retardant materials for thermoplastic polymers. J Therm Anal Calorim. 2016;127:2273–82.
13. Wu Z, Wang H, Tian X, Ding X, Xue M, Zhou H, Zheng K. Mechanical and flame-retardant properties of styrene–ethylene–butylene–styrene/carbon nanotube composites containing bisphenol A bis(diphenyl phosphate). Compos Sci Technol. 2013;82:8–14.
14. Ma H-Y, Tong L-F, Xu Z-B, Fang Z-P. Functionalizing carbon nanotubes by grafting on intumescent flame retardant: nanocomposite synthesis, morphology, rheology, and flammability. Adv Funct Mater. 2008;18:414–21.
15. Xu S, Zhang L, Lin Y, Li R, Zhang F. Layered double hydroxides used as flame retardant for engineering plastic acrylonitrile–butadiene–styrene (ABS). J Phys Chem Solids. 2012;73:1514–7.
16. Attia NF, Goda ES, Nour MA, Sabaa MW, Hassan MA. Novel synthesis of magnesium hydroxide nanoparticles modified with organic phosphate and their effect on the flammability of acrylonitrile-butadiene styrene nanocomposites. Mater Chem Phys. 2015;168:147–58.
17. Attia NF, Hassan MA, Nour MA, Geckeler KE. Flame-retardant materials: synergistic effect of halloysite nanotubes on the flammability properties of acrylonitrile-butadiene-styrene composites. Polym Int. 2014;63:1168–73.
18. Attia NF, Abd El-Aal NS, Hassan MA. Facile synthesis of graphene sheets decorated nanoparticles and flammability of their polymer nanocomposites. Polym Degrad Stab. 2016;126:65–74.
19. Du X, Yu H, Wang Z, Tang T. Effect of anionic organoclay with special aggregate structure on the flame retardancy of acrylonitrile–butadiene–styrene/clay composites. Polym Degrad Stab. 2010;95:587–92.
20. Triantou MI, Stathi KI, Tarantili PA. Thermal, mechanical, and dielectric properties of injection molded graphene nanocomposites based on ABS/PC and ABS/PP blends. Polym Compos. 2019;40:E1662–72.
21. Huang G, Huo S, Xu X, Chen W, Jin Y, Li R, Song P, Wang H. Realizing simultaneous improvements in mechanical strength, flame retardancy and smoke suppression of ABS nanocomposites from multifunctional graphene. Compos Part B Eng. 2019;177:107377.
22. Huang G, Han D, Jin Y, Song P, Yan Q, Gao C. Fabrication of nitrogen-doped graphene decorated with organophosphor and lanthanum toward high-performance ABS nanocomposites. ACS Appl Nano Mater. 2018;1:3204–13.
23. Cicero S, Sánchez M, Martínez-Mata V, Arrieta S, Arroyo B. Structural integrity assessment of additively manufactured ABS, PLA and graphene reinforced PLA notched specimens combining failure assessment diagrams and the theory of critical distances. Theor Appl Fract Mech. 2022;121:103535.
24. Wang F, Zhang Y, Zhang BB, Hong RY, Kumar MR, Xie CR. Enhanced electrical conductivity and mechanical properties of ABS/EPDM composites filled with graphene. Compos Part B Eng. 2015;83:66–74.
25. Jindal P, Goyal M, Sharma V. Preparation, characterization and study of mechanical properties of graphene/ABS nano-composites. Ind J Sci Technol. 2017;10:1–5.
26. Li P, Zheng Y, Li M, Fan W, Shi T, Wang Y, Zhang A, Wang J. Enhanced flame-retardant property of epoxy composites filled with solvent-free and liquid-like graphene organic hybrid material decorated by zinc hydroxystannate boxes. Compos Part A Appl Sci Manuf. 2016;81:172–81.
27. Wang W, Kan Y, Liu J, Liew KM, Liu L, Hu Y. Self-assembly of zinc hydroxystannate on amorphous hydrous TiO2 solid sphere for enhancing fire safety of epoxy resin. J Hazard Mater. 2017;340:263–71.
28. Wang B, Sheng H, Shi Y, Song L, Zhang Y, Hu Y, Hu W. The influence of zinc hydroxystannate on reducing toxic gases (CO, NO(x) and HCN) generation and fire hazards of thermoplastic polyurethane composites. J Hazard Mater. 2016;314:260–9.
29. Zhang X, Zhang F, Zhang W, Tang X, Fan H-JS. Enhance the interaction between ammonium polyphosphate and epoxy resin matrix through hydrophobic modification with cationic latex. Colloid Surf A. 2021;610:125917.
30. Zhang Z, Li X, Yuan Y, Pan YT, Wang DY, Yang R. Confined dispersion of zinc hydroxystannate nanoparticles into layered bimetallic hydroxide nanocapsules and its application in flame-retardant epoxy nanocomposites. ACS Appl Mater Interfaces. 2019;11:40951–60.
31. Huo Z, Wu H, Song Q, Zhou Z, Wang T, Xie J, Qu H. Synthesis of zinc hydroxystannate/reduced graphene oxide composites using chitosan to improve poly(vinyl chloride) performance. Carbohydr Polym. 2021;256:117575.
32. Di Franco F, Zaffora A, Megna B, Santamaria M. Heterogeneous crystallization of zinc hydroxystannate on galvanized steel for enhancing the bond strength at the rebar/concrete interface. Chem Eng J. 2021;405:126943.
33. Zhou H, Zhou Y, Cao Y, Wang Z, Wang J, Zhang Y, Pan W. Hollow LDH cage covering with ultra-thin MXenes veil: integrated micro-nano structure upon heat release suppression and toxic effluents elimination for polymer. Chem Eng J. 2023;461:142035.
34. Wei C, Zhang Q, Wang Z, Yang W, Lu H, Huang Z, Yang W, Zhu J. Recent advances in MXene-based aerogels: Fabrication, performance and application. Adv Funct Mater. 2022;33:2211889.
35. Zhu S-E, Wang F-D, Liu J-J, Wang L-L, Wang C, Yuen ACY, Chen TBY, Kabir II, Yeoh GH, Lu H-D, Yang W. BODIPY coated on MXene nanosheets for improving mechanical and fire safety properties of ABS resin. Compos Part B Eng. 2021;223:109130.
36. Luo Y, Xie Y, Geng W, Chu J, Wu H, Xie D, Sheng X, Mei Y. Boosting fire safety and mechanical performance of thermoplastic polyurethane by the face-to-face two-dimensional phosphorene/MXene architecture. J Mater Sci Technol. 2022;129:27–39.
37. Wan M, Shi C, Qian X, Qin Y, Jing J, Che H, Ren F, Li J, Yu B. Interface assembly of flower-like Ni-MOF functional MXene towards the fire safety of thermoplastic polyurethanes. Compos Part A Appl Sci Manuf. 2022;163:107187.
38. Zhou K, Gong K, Gao F, Yin L. Facile strategy to synthesize MXene@LDH nanohybrids for boosting the flame retardancy and

smoke suppression properties of epoxy. Compos Part A Appl Sci Manuf. 2022;157:106912.
39. Lin B, Yuen ACY, Li A, Zhang Y, Chen TBY, Yu B, Lee EWM, Peng S, Yang W, Lu HD, Chan QN, Yeoh GH, Wang CH. MXene/chitosan nanocoating for flexible polyurethane foam towards remarkable fire hazards reductions. J Hazard Mater. 2020;381:120952.
40. Peng C, Yang X, Li Y, Yu H, Wang H, Peng F. Hybrids of two-dimensional Ti3C2 and TiO2 exposing 001 facets toward enhanced photocatalytic activity. ACS Appl Mater Interfaces. 2016;8:6051–60.
41. Gao T, Sang B, Shao B, Li R, Li Z. Flame retardancy and mechanical properties of a novel zinc hydroxystannate/epoxy resin nanocomposite. J Nanosci Nanotechnol. 2017;17:8856–63.
42. Hamzah MS, Mariatti M. Properties of flame-retardant fillers in polypropylene/ethylene propylene diene monomer composites. J Thermoplast Compos Mater. 2012;26:1223–36.
43. Jiao Y, Xu JZ. Flame-retardant properties of magnesium hydroxystannate and strontium hydroxystannate coated calcium carbonate on soft poly(vinyl chloride). J Appl Polym Sci. 2009;112:36–43.
44. Liu F, Zhou X, Gao Q, Wang X, Jiao Y, Xu J. Preparation of zinc hydroxystannate coated dendritic-fibrillar barium carbonate and its flame retardant effect on soft poly (vinyl chloride). J Macromol Sci B. 2020;59:659–71.
45. Wang X, Chen T, Peng C, Hong J, Lu Z, Yuan C, Zeng B, Luo W, Dai L. Synergistic effect of mesoporous nanocomposites with different pore sizes and structures on fire safety and smoke suppression of epoxy resin. Macromol Mater Eng. 2019;305:1900640.
46. Xu W, Chen R, Xu J, Zhong D, Cheng Z. Nickel hydroxide and zinc hydroxystannate dual modified graphite carbon nitride for the flame retardancy and smoke suppression of epoxy resin. Polym Degrad Stabil. 2020;182:109366.
47. Xing W, Yang W, Yang W, Hu Q, Si J, Lu H, Yang B, Song L, Hu Y, Yuen RKK. Functionalized carbon nanotubes with phosphorus- and nitrogen-containing agents: effective reinforcer for thermal, mechanical, and flame-retardant properties of polystyrene nanocomposites. ACS Appl Mater Interfaces. 2016;8:26266–74.
48. Wu J-N, Chen L, Fu T, Zhao H-B, Guo D-M, Wang X-L, Wang Y-Z. New application for aromatic Schiff base: high efficient flame-retardant and anti-dripping action for polyesters. Chem Eng J. 2018;336:622–32.
49. Wang J, Wei Y, Wang Z, He X, Wang C, Lin H, Deng Y. MOFs-derived self-sacrificing template strategy to double-shelled metal oxides nanocages as hierarchical interfacial catalyst for suppressing smoke and toxic gases releases of epoxy resin. Chem Eng J. 2022;432:134328.
50. Sandinge A, Fredriksson H, Blomqvist P. Evaluation of smoke gas toxicity and smoke density of bus interior materials. Fire Mater. 2022;47:270–81.
51. Huang L, Zhu G, Zhang G, Yin F. Research the occupants safe egress of underground pedestrian street based on the analysis of fire smoke movement. Procedia Eng. 2013;52:158–64.
52. Long X, Zhang X, Lou B. Numerical simulation of dormitory building fire and personnel escape based on Pyrosim and Pathfinder. J Chin Inst Eng. 2017;40:257–66.
53. Zhou M, Zhou B, Zhang Z, Zhou Z, Liu J, Li B, Wang D, Wu T. Fire egress system optimization of high-rise teaching building based on simulation and machine learning. Fire. 2023;6:190.
54. Mao Y, Wang D, Hu J, Fu S. Mechanically flexible and flame retardant polyphenol-bridged casein/MXene composite for fire proofing repeatable contact/non-contact fire monitoring. Chem Eng J. 2023;454:140161.
55. Yu B, Yuen ACY, Xu X, Zhang Z-C, Yang W, Lu H, Fei B, Yeoh GH, Song P, Wang H. Engineering MXene surface with POSS for reducing fire hazards of polystyrene with enhanced thermal stability. J Hazard Mater. 2021;401:123342.
56. Chen H-R, Meng W-M, Wang R-Y, Chen F-L, Li T, Wang D-D, Wang F, Zhu S-E, Wei C-X, Lu H-D, Yang W. Engineering highly graphitic carbon quantum dots by catalytic dehydrogenation and carbonization of Ti3C2Tx-MXene wrapped polystyrene spheres. Carbon. 2022;190:319–28.
57. Yang W, Zhou Q, Pan W, Zhu S, Wei C, Lu H, Yang W, Yuen ACY. Synthesis of vanillin-based porphyrin for remarkably enhancing the toughness, UV-resistance and self-extinguishing properties of polylactic acid. Chem Eng J. 2023;469:143935.
58. Lu J, Wang B, Jia P, Cheng W, Liao C, Xu Z, Cheng L, Hu Y. Designing advanced 0D–2D hierarchical structure for epoxy resin to accomplish exceeding thermal management and safety. Chem Eng J. 2022;427:132046.
59. Lu J, Jia P, Liao C, Xu Z, Chu F, Zhou M, Yu B, Wang B, Song L. Leaf vein-inspired engineering of MXene@SrSn(OH)6 nanorods towards super-tough elastomer nanocomposites with outstanding fire safety. Compos Part B Eng. 2022;228:109425.